ADVANCED INTELLIGENT SYSTEMS
Open Access
www.advintellsyst.com

Exploiting Phase Transitions in Polymer Bilayer Actuators

*Livius F. Muff and Christoph Weder**

In many biological systems, the process of motion involves mechanically morphing materials, which change their mechanical properties and/or shape in response to a control signal. In the past two decades, significant progress has been made toward mimicking the underlying designs and resulting functions in artificial materials and systems. Polymer-based bilayer bending actuators, in which the dissimilar thermal expansion of two materials is exploited, represent widely investigated actuation elements, but one limitation of this design approach is that the thermal expansion coefficient of polymers is generally small. Herein, it is shown that this problem is mitigated using a thermoplastic polyurethane elastomer with a crystallizable soft segment. The domains formed by the latter reversibly melt and crystallize in a convenient temperature range (30–60 °C), whereas the hydrogen-bonded urethane hard segments serve as physical crosslinks that provide mechanical integrity and elastic behavior beyond this temperature. Melting the polyester results in a large nonlinear thermal expansion and thus actuation, in a narrow temperature range. The electrically controlled bilayer actuators are created by combining this material with cellulose acetate and integrating resistive heating electrodes. Optionally these devices are equipped with a thermally controlled supramolecular polymer adhesive "gripper."

Mechanically morphing materials, which change their shape and/or mechanical properties in response to a control signal, are omnipresent in nature and enable essential functions, especially in the context of (loco)motion.[1] Examples include pine cones, the desert resurrection plant, wheat awns, and the Venus fly trap.[2–6] In many cases, the material design involves hierarchical structures that efficiently translate chemical or physicochemical events from a molecular to the macroscopic level and which enable considerable mechanical effects with only minor or no compositional changes.[7] Inspired by the structure and function of such mechanically morphing biological materials,[8] and thanks to a rapidly evolving understanding of the underlying operating principles,[1] significant progress has been made in the past two decades to mimic such architectures and functions in artificial materials[9–12] and utilize these in engineering applications that range from architecture to soft robotics.[13–16] The operating principle of bioinspired polymer bilayer actuators,[17] which is similar to that of much-longer known bimetallic strips,[18] is based on the dissimilar expansion of the two components in response to an external stimulus. In contrast to bimetallic systems, in which the process is limited to thermal expansion, polymers can also expand by way of swelling, which is a process that is also at play in many biological systems. Thermal actuation of bilayer systems is not only possible by direct heating; there are many examples of actuation systems with integrated transducers that convert UV, visible, or near-infrared light, oscillating magnetic fields, or electricity into heat.[19–22]

The bending curvature of thermally controlled bilayer actuators depends on the coefficient of linear thermal expansion (CLTE) mismatch between the materials that make up the two layers,[18] and therefore polymer bilayer actuators are typically assembled from one material with a high CLTE and one material having a low CLTE. Polydimethylsiloxane (PDMS)[23–25] and low-density polyethylene (LDPE),[26–28] which both feature a high volume fraction of an expansible mobile phase, are typically used as high-thermal-expansion materials (**Figure 1**A), whereas glassy polymers, such as cellulose acetate and atactic polystyrene, can be employed as low-expansion components.[29–31] Furthermore, the mechanical characteristics of the polymers, notably their Young's moduli, and the device geometry, especially the aspect ratio and layer thickness, influence the maximum deflection, blocking force, and bending angle of simple bilayer actuators.[18] The isotropic nature of the thermally induced volume change in bilayer actuators leads a priori to biaxial bending along the long and short edges (Figure S1, Supporting Information). However, the rectangular shape of the elements investigated here favors curving of the long edge, due to the energy-lowering double curvature effect and aspect ratio.[32] Exploiting the discontinuity in volume associated with a first-order phase transition, specifically melt transition, appears to be an intriguing opportunity in the context of bilayer actuators, as this should allow one to realize a large mechanical change in a small, well-defined temperature range. Surprisingly, however, examples in which melting and crystallization events have been exploited in the context of such actuators have thus remained rare. Stroganov et al. reported confined crystallization of thin, cross-linked polycaprolactone–gelatin bilayer films in water,[33] whereas Blonder has shown that a nonlinear,

L. F. Muff, Prof. C. Weder
Adolphe Merkle Institute
University of Fribourg
Chemin des Verdiers 4, CH-1700 Fribourg, Switzerland
E-mail: christoph.weder@unifr.ch

The ORCID identification number(s) for the author(s) of this article can be found under https://doi.org/10.1002/aisy.202000177.

DOI: 10.1002/aisy.202000177

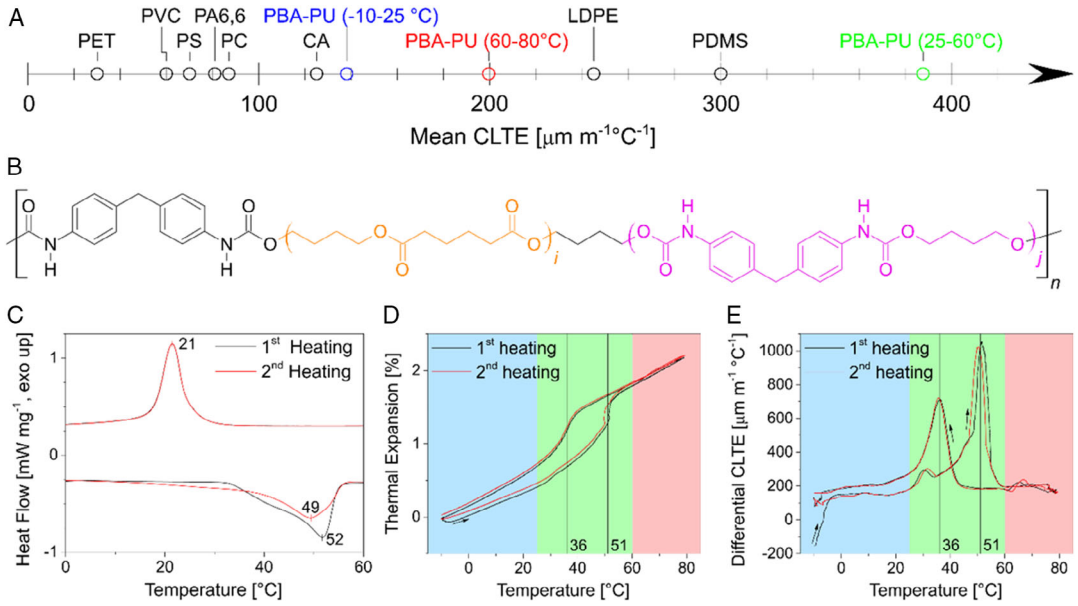

Figure 1. A) Plot showing the mean coefficient of linear thermal expansion (CLTE) of PBA-PU in different temperature regimes in comparison to the CLTE values of common polymers used as the high-thermal-expansion component of polymer bilayer actuators.[29–31] B) Chemical structure of the TPE (PBA-PU) featuring methylenediphenylisocyanate-1,4-butanediol (MDI-BD, magenta) hard segments and poly(butylene adipate) (PBA, orange) as crystallizable soft segments. C) DSC traces of a compression-molded PBA-PU film (thickness 1 mm), acquired with heating and cooling rates of 10 °C min^{-1}. D) Thermal expansion and E) differential CLTE of a compression-molded PBA-PU film (thickness 0.1 mm) measured in a dynamic mechanical analyzer with a heating rate of 0.5 °C min^{-1}. Two heating–cooling cycles were measured to eliminate thermal history of the samples.

temperature-dependent expansion can be achieved with phase-changing composites (paraffin microspheres in a polymer matrix).[34] Paraffin as high-energy-density solid–liquid phase-change material has been used to construct various actuators, valves, and pumps, but the liquid nature of paraffins in the switched state complicates the design of bilayer actuators.[35] There are many examples of bilayer actuators relying on semi-crystalline polymers such as LDPE as high-thermal-expansion material, but these do not take advantage of the polymer's melt transition, because the crystalline domains serve as physical crosslinks and their melting would compromise the device stability. Here we show that this problem can be overcome using a thermoplastic polyurethane elastomer (TPE) with a crystallizable polyester soft segment. The domains formed by the latter can be reversibly melted and crystallized in a convenient temperature range (30–60 °C), whereas the hydrogen-bonded urethane hard segments serve as physical crosslinks that provide mechanical integrity up to a much higher temperature and impart the material with rubber elasticity. Heating across the melt transition of the polyester results in a large nonlinear thermal expansion within a narrow actuation temperature range. We combined this material with cellulose acetate and integrated resistive heating electrodes, thus creating electrically controlled bilayer actuators. We additionally equipped these devices with a new type of "nonmechanical gripper" based on a thermoresponsive supramolecular polymer adhesive, which we activate using an electrical signal.

The TPE that was used as high-thermal-expansion material (PBA-PU, Figure 1A) is a modified version of a commercially available TPE,[36–42] which was prepared as previously described by Shirole et al.[43,44] The polymer features hard segments formed by the reaction of methylene diphenyl isocyanate and 1,4-butanediol (MDI-BD), which serve as physical crosslinks and poly(butylene adipate) (PBA) as the crystallizable soft segment (Figure 1B). The differential scanning calorimetry (DSC) traces match an earlier report[42] and reveal a melting transition associated with the PBA domains around a temperature (T_m) of 51 °C and a crystallization temperature (T_c) of 20–37.5 °C (Figure 1C, Figure S2, Supporting Information) depending on the cooling rate. The melting transition is broad, on account of the previously reported complex crystallization behavior of PBA,[45–51] which crystallizes in two polymorphs, the thermodynamically more stable α- and the kinetically preferred β-form. Accordingly, the morphology and thermal behavior depend somewhat on the thermal history, which explains the different profiles seen in the first and second DSC heating traces (Figure 1C). PBA-PU shows a room-temperature (20 °C) storage modulus (E') of 387 MPa, which upon heating beyond the PBA's T_m drops to 6 MPa (at 70 °C). The rubbery plateau extends to about 175 °C, where the PU's hard segments dissociate and the material liquefies (Figure S3A, Supporting Information).

Figure 1D shows the thermal expansion of PBA-PU, measured in a dynamic mechanical analyzer with a heating rate of 0.5 °C min^{-1}, as a function of temperature. Below ≈25 and above ≈60 °C, the thermal expansion of PBA-PU is linear, with mean CLTE values of 138 and 200 μm m^{-1} °C^{-1}, respectively (Figure 1D, areas shaded blue and red). The increased CLTE in the higher-temperature regime is a consequence of the higher fraction of mobile chain segments upon melting of the PBA domains. Figure 1D also clearly shows the "nonlinear" expansion behavior associated with the melting and crystallization of the

PBA domains in the temperature range of 25–60 °C, reflected by slope changes and clear discontinuities at around 51 °C upon heating and 36 °C upon cooling. The discontinuous expansion just around T_m (≈0.32% between 50 and 52 °C) corresponds to about one-quarter of the total thermal expansion in the actuation range (≈1.4% between 20 and 60 °C). The mean CLTE in the temperature range of 25–60 °C is 388 μm m^{-1} °C^{-1} and thus much larger than that of other polymers used in bilayer actuators (Figure 1A). The differential CLTE (Figure 1E) shows a maximum of 1025 μm m^{-1} °C^{-1} at T_m (51 °C) and a local maximum around 32 °C, which is associated with the formation of small α-form crystals. Taken together, the data reflect strikingly that PBA-PU exhibits a very large thermal expansion in a narrow temperature regime. Although the broad melting transition, complex crystallization behavior, rather low crystallinity, and appreciable difference between T_m and T_c of the PBA domains are all aspects that leave room for improvement, PBA-PU still outperforms other common polymers (Figure 1A) in terms of CLTE and demonstrates that the use of phase-change materials in soft actuators can be advantageous.

To fabricate bilayer actuators (**Figure 2**A), PBA-PU was combined with cellulose acetate (CA) as the low-thermal-expansion component (mean CLTE = 78 μm m^{-1} °C^{-1} in the range of 0–100 °C, Figure S4, Supporting Information). The glassy CA exhibits a high Young's modulus (≈1.7 ± 0.1 GPa at 20 °C, Figure S3C, Supporting Information) and an appreciable tensile strength (≈65 ± 16 MPa at 20 °C, Figure S3C, Supporting Information) and thanks to the high glass transition temperature (T_g) of 190 °C these characteristics are retained in a broad temperature range, so that the CA layer provides strength and stiffness above T_m of the PBA domains, while being flexible enough to permit the bending motion of the bilayer actuator (vide infra).[52] CA was compression molded into films of a thickness of 300 μm, onto which a 100 nm-thick gold electrode was applied via physical vapor deposition (PVD) through a mask (Figure S5, Supporting Information) to serve as a Joule heater and enable electrically controlled actuation. PBA-PU was either directly compression molded onto the CA film or separately compression molded into a film and subsequently joined with the CA film by adhesive bonding, using a commercial PDMS-based adhesive. The bilayer films thus created were cut around the imprinted heating electrode pattern into actuators with lateral dimensions of ≈25 × 65 mm (Figure 2B). The optimal PBA-PU layer thickness (300 μm) was calculated based on Timoshenko's bilayer deflection model (Equation S1, Supporting Information)[18] with the goal of maximizing the bilayer bending curvature (Figure S6, Supporting Information). Compression-molded bilayer actuators (Figure 2C, top) are bent in the idle state, due to shrinkage of the PBA-PU layer upon cooling to ambient temperature, which is in part caused by the crystallization of the PBA domains. These bilayer actuators bend toward the CA layer and thus flatten when heated above the PBA T_m and return to their bent state upon cooling to ambient temperature. Adhesively bonded bilayer actuators (Figure 2C, bottom) assume a flat idle state at ambient temperature and, also bending toward the CA layer, transition into a curved conformation above the PBA T_m.

The deposited gold electrodes (channel width: 2 mm, thickness: 100 nm), when sandwiched between the CA and PBA-PU layers, show a typical resistance of 35 Ω. The heating power generated by applying a voltage can be calculated with the

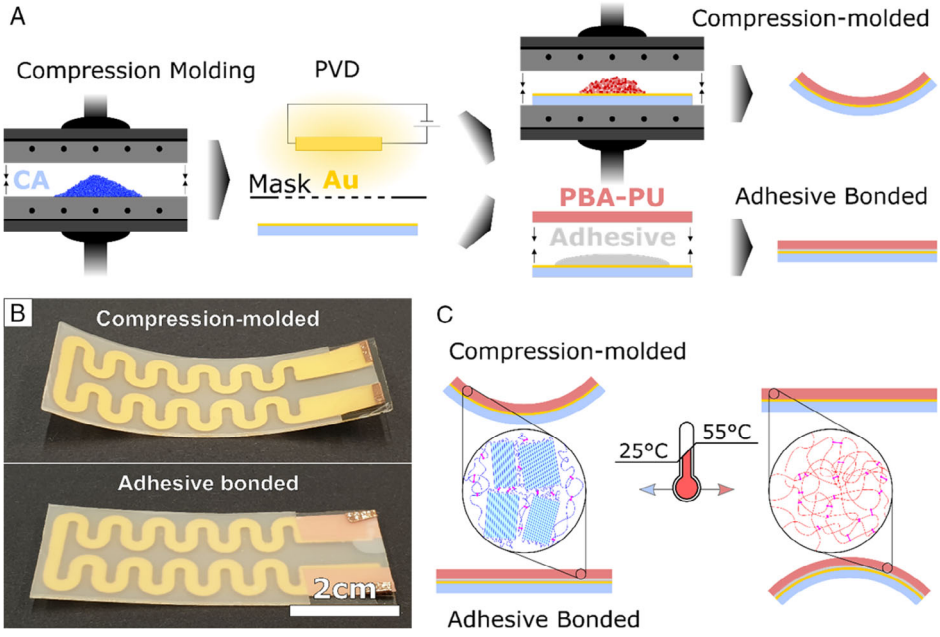

Figure 2. A) Schematic showing the different fabrication approaches and architecture of PBA-PU/CA bilayer actuators. PBA-PU (red) was either directly compression molded (top) onto a CA (blue) film (1 min, 180 °C, 4 t) or PBA-PU and CA films were separately made and bonded with a PDMS-based adhesive (gray, bottom). In both cases, a mask was used to pattern a resistive gold heating electrode of a thickness of 100 nm onto the CA film by PVD. B) Pictures of bilayer actuators fabricated by compression molding (top) and adhesive bonding (bottom), taken in ambient conditions. The bilayer actuators (25 × 65 × 0.6 mm) feature a 2 mm-wide and 100 nm-thick gold Joule heating electrode. C) Schematics of the bending states of the two actuator types at ambient temperature (left) and above the actuation temperature, the T_m of PBA (right).

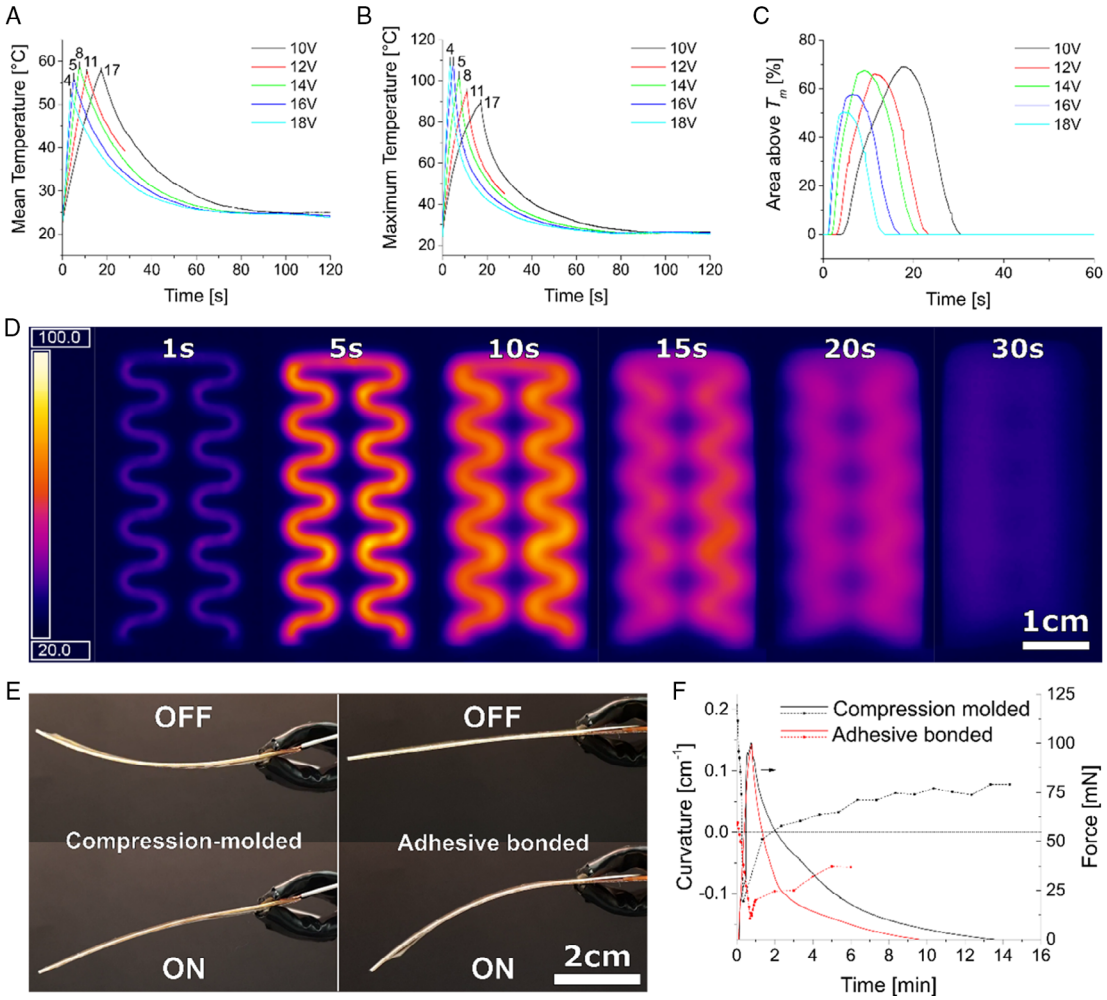

Figure 3. A–C) Temperature–time traces of a compression-molded PBA-PU/CA bilayer actuator that was operated by applying voltages of 10–18 V. Plotted are the A) mean temperature, B) maximum temperature, and C) the area percentage of PBA-PU melted (heated above 50 °C). D) Infrared (IR) thermographic images of a compression-molded PBA-PU/CA bilayer actuator after various operation times with an applied voltage of 14 V. E) Pictures showing compression-molded and adhesively bonded PBA-PU/CA bilayer actuator before and after actuation. F) Blocking force (solid lines) and curvature traces (dotted lines) for compression-molded and adhesively bonded bilayer actuators during one actuation cycle. Both devices were operated with an applied voltage of 14 V.

generalized power equation ($P = V^2/R$). **Figure 3**A shows the mean temperature of a compression-molded PBA-PU/CA bilayer actuator during one actuation cycle at different operating voltages of 10–18 V, which translate into powers of 2.9–9.3 W. The peak seen in the time-temperature graphs marks the time point when the actuator reached its flat state and voltage was turned off. The data show that a higher operating voltage (and thus power) leads to faster actuation at a similar "mean" temperature of 54–58 °C. However, the evolution of the maximal actuator temperature (Figure 3B) indicates that higher power also leads to larger temperature gradients within the actuator, which in turn causes inhomogeneous melting of the PBA-PU layer. A plot of the percentage of melted PBA-PU versus actuation time (Figure 3C) shows that when actuation is achieved at a higher voltage, significantly less PBA-PU is melted (≈50% at 18 V) compared with lower voltage (≈70% at 10 V) to achieve actuation. Therefore, at a lower operating voltage, actuation depends on a larger melted PBA-PU area, making thermal transport within the bilayer actuator a dominating factor for actuation time. The result is a reduced temperature required for actuation but a longer actuation time (Figure 3A). To mitigate this, the heating electrode was designed to feature a large contact area with the PBA-PU layer to achieve homogeneous heating (Figure S5, Supporting Information). Thermal imaging of a compression-molded actuator under applied voltage (14 V, Figure 3D) reveals how heat travels from the Joule heater through the PBA-PU layer. The images show that even after actuation at 8 s, the temperature of the bilayer is not homogeneous (10–30 s). This is also the case for lower (10 and 12 V) and higher (16 and 18 V) applied voltages (Figure S7, Supporting Information), indicating that thermal transport affects the PBA-PU/CA bilayer actuators regardless of the applied voltage. As part of a future design, a more elaborate heating electrode with increased contact area could potentially overcome this problem and further improve the actuation performance.[53]

As mentioned earlier, the compression-molded PBA-PU/CA bilayer actuators are bent at room temperature due to the crystallization-enhanced contraction of the PBA soft segment upon cooling to ambient temperature after melt processing. When a sufficiently large fraction of the PBA crystalline phase has melted, the stored tension is released and the bilayer snaps into its flat state, similar to the way in which a bow releases an arrow (Figure 3E, left, Supporting Movie 1, Supporting Information). In contrast, adhesively bonded bilayer actuators are flat at ambient temperature and show a continuous bending motion upon heating, due to thermal expansion of the PBA soft segment (Figure 3E, right, Supporting Movie 2, Supporting Information). The corresponding blocking force traces reveal that both bilayer actuator types have a maximum blocking force of 100 mN (Figure 3F). The compression-molded bilayers initially show a limited force buildup (25 mN), which is followed by an instantaneous force increase as the PU-PBA layer softens enough to release the energy stored in the bent CA layer. As the temperature is increased further, the blocking force continues to build up until heating stops after 30 s. This gradual increase in the blocking force throughout actuation is more linear for the adhesively joined actuators than for the compression-molded bilayers. Upon cooling, the blocking force decreases faster in the case of the adhesively bonded bilayer actuator, as the CA layer acts like a spring and assists the bilayer into its flat resting state. For the compression-molded bilayer, the recovery is slower, because the contracting PBA-PU layer must bend the stiff CA layer and because the crystallization of the PBA soft segment is inherently slow. Curvature traces show that a large curvature change ($0.35\ cm^{-1}$) is possible for the compression-molded bilayer actuators, as these devices can continue to bend beyond their flat state. The mechanically resisting CA layer allows for bending at around $0.20\ cm^{-1}$ in both directions.

To demonstrate the functionality of the actuators reported here, we built a soft robotic arm by joining two compression-molded PBA-PU/CA bilayer actuators perpendicularly along their short edges using a thermoformed piece of CA (**Figure 4**A, S8A, Supporting Movie 3, Supporting Information). The two elements were independently controlled via integrated heating electrodes as reported earlier and an additional electrode was applied at the end of the front actuator (Figure S5, Supporting Information) that was used to activate a thermo-responsive "gripper." This element was based on ≈1 × 2 × 1 mm-sized film of supramolecular adhesive based on acrylated epoxidized soybean oil–isophthalic acid (AESO-IPA).[54] The sequence of images shown in Figure 4 and Supporting Movie 3, Supporting Information, shows that it is possible to pick up, move, and drop an object of considerable weight (0.5 g) by applying the sequence of 1) liquefying the thermo-responsive adhesive by heating the gripper element to 70 °C, 2) lowering the arm and contacting the object by activating the front actuator, 3) bonding the object by switching off the gripper element and solidifying the thermo-responsive adhesive, 4) lifting the object by switching off the front actuator and raising the arm by allowing it to passively recover, 5) sideways movement by activating the back actuator, and 6) releasing the object by activating the gripper element again. In particular the passive recovery step is quite slow; the T_c of the PBA-PU is close to ambient temperature, which makes the crystallization of the PBA domains upon cooling a slow process. However, we note that this limitation can be addressed by minimizing the T_m–T_c gap and thereby the resulting hysteresis loop (Figure 1C,D), by creating a similar TPE with a more rapidly crystallizing soft segment.

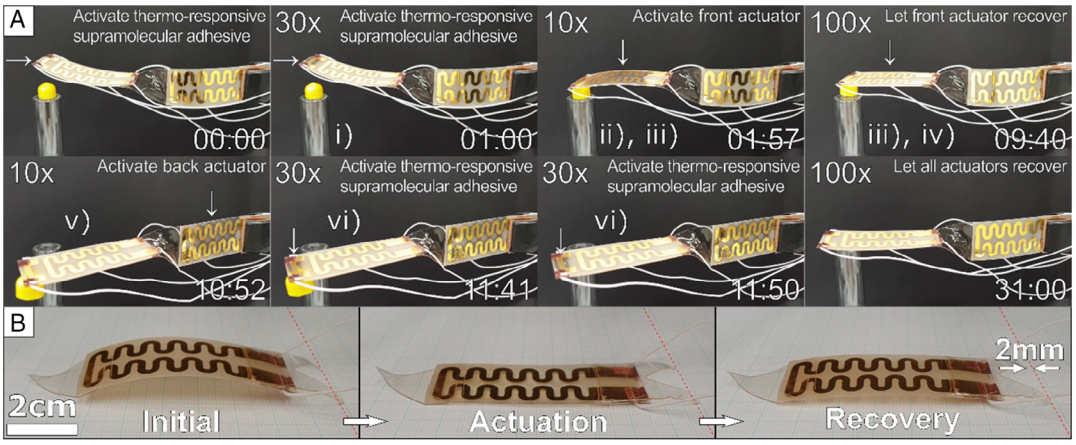

Figure 4. A) Picture series showing two individually controlled compression-molded PBA-PU/CA bilayer actuators joined perpendicular to each other with a thermoformed CA piece (Figure S8A, Supporting Information) to form a soft robotic arm. An additional smaller electrode at the end of the front actuator was integrated to control a film (1 × 2 × 0.1 mm) of thermo-responsive adhesive (AESO-IPA),[54] which allows temporary adhesion to objects and thus acts as a thermally controlled gripper. i) The front heating electrode is powered to liquefy the thermoresponsive adhesive (70 °C). ii) By powering the front bilayer bending actuator, the arm is lowered and contacts the yellow object (0.5 g). iii) Switching off the gripper element solidifies the thermo-responsive adhesive and binds the object to the soft robotic arm. iv) The object is lifted by switching off the front actuator, allowing it to passively recover. v) Heating the back actuator moves the bonded object sideways. vi) The yellow object is released by powering the gripper heating electrode again. Finally, the soft robotic arm passively recovers to its original position. All integrated Joule heaters were operated with 14 V. B) Pictures show a compression-molded PBA-PU/CA bilayer actuator equipped with thermoformed CA elements to imitate inchworm locomotion. Upon actuation (14 V) the low friction side is pushed forward while the anchor points keep the other end in place. During recovery, the anchor points are released and dragged across the paper as the actuator bends. The artificial inchworm advances ≈2 mm per heating and recovery cycle.

We also equipped a melt-processed PBA-PU/CA bilayer actuator with thermoformed CA ends (Figure S8B, Supporting Information) to explore inchworm-inspired locomotion (Figure 4B). Upon actuation, the low-resistance curved front is pushed forward, with the two pointy ends acting as anchors on the paper substrate. During recovery, the actuator starts to bend and releases the anchor points, which are then dragged toward the front. The artificial inch worm was able to travel an average distance of 2 mm per actuation cycle (heating and recovery).

In summary, we have shown that the first-order (melt) transition in a TPE that features, in addition to the urethane hard segments, a crystallizable soft block can display a large nonlinear thermal expansion coefficient in a narrow temperature regime without melting and demonstrated that materials with such a property combination are a priori useful for the fabrication of actuators. Bilayer actuators with CA produced by compression molding are bent in a resting state, as a result of dissimilar shrinkage of the two materials upon cooling. These actuators snap into a flat state upon actuation as the tension of the bent CA layer is released instantaneously once enough PBA soft segment is molten. Adhesively bonded bilayer actuators rest in flat geometry and bend continuously during actuation due to thermal expansion of the PBA-PU layer and melting of the PBA soft segment. In the devices reported here, full actuation was achieved within 7 s; because the response was limited by thermal transport through the bilayer, even faster response times appear feasible through improved electrode design. The slow recovery is caused by the relatively large difference between melting and crystallization temperature and the fact that crystallization is close to ambient temperature. Thus, the next-generation material for these types of bilayer bending actuators should be designed to feature sharper transitions and a more narrow gap between melting and crystallization, which can to a certain extent be achieved by nucleating the PBA-PU crystallization[43,44] or replacing the PBA with a polyolefin soft segment.[35] We have also introduced a thermally controlled supramolecular polymer adhesive "gripper," which constitutes another novel design experiment in soft robotics. This element adds compelling functionality to the already established electrothermally operated actuator platform and should be compatible with a wide variation of the existing electrothermal soft robotic devices.

Experimental Section

Compression Molding: A bench-top manual press with electrically heated platens (Model 4386) from Carver Inc. was used to prepare polymer films and compression-molded bilayer actuators. CA films ($M_n \approx 30$ kDa by GPC obtained from Sigma Aldrich [180955-500G] in powder form) were produced by compression molding the as-received CA for 1 min at 235 °C under 4 t load between two Kapton sheets (thickness: 60 μm) using stainless steel spacers to obtain 300 μm (for bilayers) and 250 μm (for thermal expansion measurements) thick films. The hot CA films between the Kapton sheets (thickness: 60 μm) were transferred and cooled between steel inserts at room temperature under a load of 5 kg for 3 min. Compression-molded CA films were stored for at least 24 h in ambient conditions before use.

PBA-PU films were produced by compression molding the as-received PBA-PU (corresponding to the melt-processed blend of Desmopan DP 2795 A with 20% w/w PBA reported by Shirole et al.)[43] obtained from Covestro Germany AG for 1 min at 180 °C under 4 t load between two Teflon sheets (thickness: 150 μm) using stainless steel spacers to obtain 100 μm (for thermal expansion measurement), 300 μm (for bilayer actuators), and 1 mm (for DSC measurements)-thick films. For compression-molded bilayers, PBA-PU granules were directly pressed onto a previously prepared CA film (thickness: 300 μm) to obtain a 600 μm-thick PBA-PU/CA bilayer. Compression-molded PBA-PU films or PBA-PU/CA bilayers were left to cool between the Teflon sheets without additional load at room temperature for at least 30 min to ensure complete crystallization of the PBA soft segment. The PBA-PU films and PBA-PU/CA bilayers were stored for at least 24 h in ambient conditions before use.

Adhesive Joining: PBA-PU and CA films (thickness: 300 μm) were joined with a PDMS-based adhesive (Pattex 100%) and cured for 24 h in ambient conditions under a 5 kg load (corresponding to a pressure of 10 kPa). A manual weighted roller (3 kg) was used to ensure homogenous adhesive thickness throughout the whole bilayer.

Physical Vapor Deposition: A MiniLab ST080M Thermal Evaporation system from Moorfield Nanotechnology Limited was used to evaporate a gold (99.99%) target from Kurt J. Lesker Company onto a previously prepared CA film covered with a laser-cut stainless steel patterning mask (Figure S5, Supporting Information) under constant rotation. Gold was typically deposited with a current of 22 A in a vacuum of 10^{-6} mbar to form a 100 nm-thick gold layer, as measured with a quartz crystal microbalance. The resistance of the patterned electrode was typically around 35 Ω.

Actuator Fabrication: Compression-molded or adhesive bonded bilayers were cut with a razor blade around the integrated heating electrode (Figure S5, Supporting Information) to obtain 25 × 65 mm-sized bilayer actuators. Conductive copper tape (width: 6 mm) was used to connect copper wires (diameter: 1 mm) to the gold connection pads of the resistive heating electrode sandwiched between the PBA-PU and CA layer. This was achieved by carefully separating the two layers with a razor blade at the connection pad.

Differential Scanning Calorimetry: DSC traces were measured with a STAR system from Mettler Toledo in nitrogen atmosphere. A sample amount of ≈5 mg was measured from −10 to 80 °C with a heating and cooling rate of 10 °C min^{-1} unless stated otherwise. Measured heat flow was divided by the sample weight, and melting (T_m) and crystallization temperature (T_c) were determined by taking the maxima of the melting endotherm and cooling exotherm.

Thermal Expansion Measurements: Thermal expansion was measured on a dynamic mechanical analyzer (Q800) from TA Instruments. The measurements were carried out following ASTM E831-06 with lower-than-suggested heating and cooling rates (0.5 °C min^{-1}) for better resolution.

Curvature Analysis: Bilayer curvatures were quantified by image analysis with FIJI using the Kappa plugin. Based on photographs, curves were manually traced with an open basic spline (B-spline) function and subsequently fitted using the least square method to account for human error.

Actuator Operation: The operating voltage and current were controlled with a Model 2400 Series source meter from Keithley. Voltages between 10 and 18 V were applied to control the Joule heaters (35 Ω) of bilayer bending actuators. For the soft robotic arm (Figure 4A), both the bending actuators and the thermoresponsive "gripper" heating element were controlled manually (14 V). For the inchworm-inspired robot (Figure 4B), the voltage (14 V) was automatically controlled with a computer connected via serial interface to the source meter to go through multiple heating and recovery cycles automatically.

Temperature–Time Traces: The maximum temperature, mean temperature, and area above 50 °C were recorded for the whole PBA-PU surface area of the bilayer actuators with a PI 160 infrared (IR) camera from Optris GmbH. The data were evaluated in the Optris PI connect software and visualized with the Origin software from OriginLab Corporation.

Blocking Force: The blocking force of the bilayer actuators was measured with an MS Semi-Micro NewClassic benchtop balance from Mettler-Toledo AG. Actuators were oriented such that they would press onto the force transducer of the microbalance during operation. The apparent weight was recorded with a computer through a serial interface and multiplied with the gravitational constant (9.8 ms^{-2}) to obtain the blocking force.

Dynamic Modulus: The mechanical properties were measured on a dynamic mechanical analyzer (Q800) from TA Instruments. Compression-molded PBA-PU stripes (width: 5.35 mm, thickness: 0.2 mm) were measured at 1 Hz with an amplitude of 15 μm from −50 to 200 °C. Reported data were extracted from a representative curve (Figure S3A, Supporting Information).

Tensile Testing: Tensile measurements were carried out according to ASTM D882, in ambient conditions, with a static material testing machine from Zwick/Roell equipped with a 200 N Xforce HP load cell. Reported data represented the average of seven ($N = 7$) independent measurements. Compression-molded PBA-PU dog bone samples (width: 4.75 mm, thickness: 0.2 mm) were measured at a strain rate of 500 mm min^{-1}. Stripes of compression-molded CA (width: 5.5 mm, thickness: 0.3 mm) were measured at a strain rate of 5 mm min^{-1}.

Optical Microscopy: Cross-polarized microscopy images were acquired with a BX51 microscope from Olympus equipped with a DP72 digital acquisition camera using the Stream Basic software suite.

Photography and Videos: Macroscopic photos and videos were taken with a Nikon D7100 digital camera equipped with an AF-S DX Zoom-NIKKOR 18–135 mm lens (f/3.5-5.6G IF-ED) and a SM-G965F mobile phone camera from Samsung.

Supporting Information

Supporting Information is available from the Wiley Online Library or from the author.

Acknowledgements

The authors gratefully acknowledge financial support from the Swiss National Science Foundation (SNSF) through the Partnerships for International Research and Education (PIRE) program under grant number IZPIP0_177995 and the Adolphe Merkle Foundation. They are also indebted to Dr. Feyza Karasu for kindly providing the mechanical data of the TPE.

Conflict of Interest

The authors declare no conflict of interest.

Keywords

bending actuators, bilayers, phase transitions, soft robotics

Received: July 27, 2020
Revised: August 31, 2020
Published online: October 5, 2020

[1] L. Montero De Espinosa, W. Meesorn, D. Moatsou, C. Weder, *Chem. Rev.* **2017**, *117*, 12851.
[2] W. M. Harlow, W. A. Côté, A. C. Day, *J. For.* **1964**, *62*, 538.
[3] C. Dawson, J. F. V. Vincent, A.-M. Rocca, *Nature* **1997**, *390*, 668.
[4] A. Rafsanjani, V. Brulé, T. L. Western, D. Pasini, *Sci. Rep.* **2015**, *5*, 8064.
[5] R. Elbaum, L. Zaltzman, I. Burgert, P. Fratzl, *Science* **2007**, *316*, 884.
[6] Y. Forterre, J. M. Skotheim, J. Dumais, L. Mahadevan, *Nature* **2005**, *433*, 421.
[7] J. U. Schmied, H. Le Ferrand, P. Ermanni, A. R. Studart, A. F. Arrieta, *Bioinspiration Biomimetics* **2017**, *12*, 026012.
[8] A. R. Studart, *Angew. Chemie Int. Ed.* **2015**, *54*, 3400.
[9] *Soft Actuators: Materials, Modeling, Applications, and Future Perspectives*, 2nd ed. (Eds: K. Asaka, H. Okuzaki), Springer Nature, Singapore **2019**.
[10] K. M. Herbert, S. Schrettl, S. J. Rowan, C. Weder, *Macromolecules* **2017**, *50*, 8845.
[11] L. Ionov, *Langmuir* **2015**, *31*, 5015.
[12] Q. Li, *Intelligent Stimuli-Responsive Materials : From Well-Defined Nanostructures to Applications*, John Wiley & Sons, Hoboken, NJ **2013**.
[13] S. Poppinga, C. Zollfrank, O. Prucker, J. Rühe, A. Menges, T. Cheng, T. Speck, *Adv. Mater.* **2018**, *30*, 1703653.
[14] S. Kim, C. Laschi, B. Trimmer, *Trends Biotechnol.* **2013**, *31*, 287.
[15] W. Hu, G. Z. Lum, M. Mastrangeli, M. Sitti, *Nature* **2018**, *554*, 81.
[16] L. Hines, K. Petersen, G. Z. Lum, M. Sitti, *Adv. Mater.* **2017**, *29*, 1603483.
[17] E. Reyssat, L. Mahadevan, *J. R. Soc. Interface* **2009**, *6*, 951.
[18] S. Timoshenko, *J. Opt. Soc. Am.* **1925**, *11*, 233.
[19] H. Kim, H. Lee, I. Ha, J. Jung, P. Won, H. Cho, J. Yeo, S. Hong, S. Han, J. Kwon, K.-J. Cho, S. H. Ko, *Adv. Funct. Mater.* **2018**, *28*, 1801847.
[20] Y. Hu, Z. Li, T. Lan, W. Chen, *Adv. Mater.* **2016**, *28*, 10548.
[21] H. K. Bisoyi, Q. Li, *Chem. Rev.* **2016**, *116*, 15089.
[22] M. Yang, Z. Yuan, J. Liu, Z. Fang, L. Fang, D. Yu, Q. Li, *Adv. Opt. Mater.* **2019**, *7*, 1900069.
[23] Q. Li, C. Liu, Y. H. Lin, L. Liu, K. Jiang, S. Fan, *ACS Nano* **2015**, *9*, 409.
[24] Y. Hu, J. Liu, L. Chang, L. Yang, A. Xu, K. Qi, P. Lu, G. Wu, W. Chen, Y. Wu, *Adv. Funct. Mater.* **2017**, *27*, 1704388.
[25] W. Zhang, M. Weng, P. Zhou, L. Chen, Z. Huang, L. Zhang, C. Liu, S. Fan, *Carbon* **2017**, *116*, 625.
[26] L. Li, J. Meng, C. Hou, Q. Zhang, Y. Li, H. Yu, H. Wang, *ACS Appl. Mater. Interfaces* **2018**, *10*, 15122.
[27] O. Kim, S. J. Kim, M. J. Park, *Chem. Commun.* **2018**, *54*, 4895.
[28] M. Yamada, M. Kondo, R. Miyasato, Y. Naka, J. I. Mamiya, M. Kinoshita, A. Shishido, Y. Yu, C. J. Barrett, T. Ikeda, *J. Mater. Chem.* **2009**, *19*, 60.
[29] J. E. Mark, *Polymer Data Handbook*, Oxford University Press, New York, NY, **2009**.
[30] G. W. Ehrenstein, G. Riedel, P. Trawiel, *Thermal Analysis Of Plastics*, Carl Hanser Verlag GmbH & Co. KG, München **2004**.
[31] H. F. Mark, *Encyclopedia Of Polymer Science And Technology*, John Wiley & Sons, Hoboken, NJ **2004**.
[32] S. Alben, B. Balakrisnan, E. Smela, *Nano Lett.* **2011**, *11*, 2280.
[33] V. Stroganov, M. Al-Hussein, J. U. Sommer, A. Janke, S. Zakharchenko, L. Ionov, *Nano Lett.* **2015**, *15*, 1786.
[34] G. Blonder, *Mater. Res. Express* **2017**, *4*, 065704.
[35] S. Ogden, L. Klintberg, G. Thornell, K. Hjort, R. Bodén, *Microfluid. Nanofluidics* **2014**, *17*, 53.
[36] R. Loewe, P. Krueger, M. Knebel, J. Ehreke, H. Pudleiner, M. Yesildag, K. Meyer, D. Pophusen, J. Buechner, US 2011/0274883 A1 **2011**.
[37] H. Pudleiner, K. Meyer, J. Winkler, W. Bräuer, J. Nickel, P. Craig, C. Li, Y. Chen, U.S. Patent 10,286,635 **2015**.
[38] R. Bouaziz, F. Roger, K. Prashantha, *Smart Mater. Struct.* **2017**, *26*, 055009.
[39] M. Ecker, T. Pretsch, *RSC Adv.* **2014**, *4*, 46680.
[40] M. Bothe, F. Emmerling, T. Pretsch, *Macromol. Chem. Phys.* **2013**, *214*, 2683.
[41] N. Mirtschin, T. Pretsch, *RSC Adv.* **2015**, *5*, 46307.
[42] N. Fritzsche, T. Pretsch, *Macromolecules* **2014**, *47*, 5952.
[43] A. Shirole, C. U. Perotto, S. Balog, C. Weder, *ACS Appl. Mater. Interfaces* **2018**, *10*, 24829.
[44] A. Shirole, A. Nicharat, C. U. Perotto, C. Weder, *Macromolecules* **2018**, *51*, 1841.
[45] R. Minke, J. Blackwell, *J. Macromol. Sci. B* **1979**, *16*, 407.
[46] R. Minke, J. Blackwell, *J. Macromol. Sci. B* **1980**, *18*, 233.
[47] P. Pan, Y. Inoue, *Prog. Polym. Sci.* **2009**, *34*, 605.

[48] Z. Gan, H. Abe, Y. Doi, *Macromol. Chem. Phys.* **2002**, *203*, 2369.
[49] Z. Gan, K. Kuwabara, H. Abe, T. Iwata, Y. Doi, *Biomacromolecules* **2004**, *5*, 371.
[50] E. M. Woo, M. C. Wu, *J. Polym. Sci. B Polym. Phys.* **2005**, *43*, 1662.
[51] M. Wang, K. Tashiro, Y. Ozaki, *Macromolecules* **2017**, *50*, 3883.
[52] L. Liu, G. Khang, J. M. Rhee, H. B. Lee, *Korea Polym. J.* **1999**, *7*, 289.
[53] H. Lu, M. Lei, C. Zhao, Y. Yao, J. Gou, D. Hui, Y. Q. Fu, *Compos. B Eng.* **2015**, *80*, 37.
[54] A. del Prado, D. K. Hohl, S. Balog, L. M. de Espinosa, C. Weder, *ACS Appl. Polym. Mater.* **2019**, *1*, 1399.